RSC Advances

ARTICLE

A facile low temperature route to deposit TiO_2 scattering layer for efficient dye-sensitized solar cells

Received 00th January 20xx,
Accepted 00th January 20xx

DOI: 10.1039/x0xx00000x

www.rsc.org/

Zahra Andaji Garmaroudi[a, †], Mojtaba Abdi-Jalebi[b, †, *], Mohammad Reza Mohammadi[a, *] and Richard H. Friend[b]

Herein, we demonstrate a facile low temperature chemical bath deposition approach to deposit a light scattering layer on a nanostructured mesoporous TiO_2 bottom layer in dye-sensitized solar cell architecture. Large TiO_2 nanoparticles were formed on the top surface of photoanode electrodes via hydrolysis of $TiCl_4$ at 70 °C. We controlled the size and agglomeration of these TiO_2 nanoparticles by altering the concentration of $TiCl_4$ in the chemical bath during the hydrolysis process. Electron microscope images revealed that mono-dispersed scattering particles having uneven surfaces with diameter between 100 to 300 nm formed on the mesoporous titania layer. The scattering behavior of the formed titania overlayer were confirmed by the improved reflectance in the diffuse reflectance spectrum of the films. We also observed a significant improvement in the density of states near the band-edge of titana for the $TiCl_4$ treated electrodes as well as a considerable decline in the sub band gap absorption states. Consequentially, enhancement in the photovoltaic parameters of $TiCl_4$ treated based solar cells is achieved which lead to a power conversion efficiency of 8.54% for the cell having an optimum content of large titania particles on the top surface compare to 7.10% for the pristine titania based solar cell.

Introduction

Dye-sensitized solar cells (DSCs) are developed as a promising alternative to commercial solar cells with the advantage of low cost[1,2]. In addition, ease of fabrication, their aesthetically pleasing colour and tunable shape make them become effective energy conversion devices which can be widely used as smart windows in building integrated photovoltaics system, portable energy convertors in the fields of wearable electronics and so forth[3–5]. A typical DSC is a sandwich of a nanocrystalline TiO_2 photoanode sensitized with dye molecules and a catalyst-coated counter electrode, with a redox electrolyte in-between. Among conventional metal oxides, TiO_2 and ZnO have been explored extensively in different nanoarchitectures and crystallographic phases[6–11]. An optimized photoanode fabricated from multi layers of different sized particles based on anatase TiO_2 have displayed the best performance to date[12]. Applying submicron-size TiO_2 particles as light scattering centers or light reflection layer on the top surface of the photoanode has been reported to be an effective approach to enhance the light harvesting in DSCs[13–16]. Coating a light-scattering layer on top of a nanoparticle layer has been introduced as an essential step in DSC fabrication processes as tiny nanoparticles exhibit high transparency to incident sunlight while scattering centers would largely increase the optical pathways inside the mesoporous film[17–20]. However, synthesizing and coating light scattering centers on a mesoporous titania layer is not a cost-effective technique as the scattering layer is formed at high temperature which adds an additional heating process[21].

In this work, we employ a facile low-temperature chemical bath deposition method to deposit a designed film of larger TiO_2 particles covering the nanocrystalline TiO_2 film as a light scattering layer to fabricate photoanode for efficient DSCs. Scanning electron microscope (SEM) images show that monodisperse large titania particles formed on the top surface of nanocrystalline TiO_2 by controlling the concentration of $TiCl_4$ in the chemical bath. X-ray diffraction (XRD) spectroscopy confirms the crystalline phases of the deposited titania layers. Diffuse reflectance spectroscopy (DRS) illustrates the improvement in the light scattering of titania electrodes which were treated with $TiCl_4$. We also did photothermal deflection optical absorption spectroscopy (PDS) to explore the effect of the $TiCl_4$ treatment on absorption spectra, density of states and the level of electronic disorder on the mesoporous titania layer. In addition, electrochemical impendence spectroscopy (EIS) was used to characterize the influence of this treatment on the charge transport properties within a complete device. Finally, fabrication of solar cells based on the photoanodes having been treated with $TiCl_4$ in different concentrations was performed in order to investigate potential impacts of controlled $TiCl_4$ post treatment on the photovoltaic parameters of the cell.

[a] Department of Materials Science and Engineering, Sharif University of Technology, Azadi Street, Tehran, Iran.
[b] Cavendish Laboratory, Department of Physics, University of Cambridge, JJ Thomson Avenue, Cambridge CB3 0HE, UK.
E-mail: ma571@cam.ac.uk, mohammadi@sharif.edu
† These authors contributed equally to this work.
Electronic Supplementary Information (ESI) available: [Transmission electron microscope images and XRD patterns of synthesized titania]. See DOI: 10.1039/x0xx00000x

Results and discussion

In this study, we synthesized mesoporous titania nanoparticles with particle size in the range of 15–30 nm with anatase crystal structure using a modified process analogous to the procedure reported previously[14]. We then employed a controlled chemical bath deposition process in a $TiCl_4$ solution in order to produce a scattering layer on top of the mesoporous TiO_2 layer. We explored four different concentrations of $TiCl_4$ in the chemical bath including 100mM (TC100), 200mM (TC200), 300mM (TC300) and 400mM (TC400). After dye loading step, the TiO_2 electrodes were coupled with a redox electrolyte and a Platinum-coated counter electrode, to complete the cell architecture (see experimental section).

Morphological and structural characterization

To understand the morphology of the synthetized mesoporous TiO_2 nanoparticles and the deposited scattering layer, transmission electron microscope (TEM) and scanning electron microscope (SEM) were used. Figure S1 shows the TEM images of the synthesized mesoporous TiO_2 nanoparticles having spherical particles with an average crystallite size of 5±1 nm. Figure 1 shows SEM images of titania overlayer formed by chemical bath deposition using $TiCl_4$ solutions with concentrations in the range from 100 to 400 mM. Using 100 and 200 mM $TiCl_4$ concentrations create a thin layer of titania on the top surface of the mesoporous layer (Figures 1b,c). Increasing the concentration up to 300 mM led to the formation of scattered large particles with an average diameter of 200 nm on the top surface (Figure 1d). Further increase in $TiCl_4$ concentration led to a higher density of bigger particle on the top surface while the size of the particles remained the same (Figure 1e).

Importantly, the XRD measurements shown in the Figure S2 reveals that the mesoporous titania layer composed of the anatase phase while the rutile phase is dominant for the top titania layer synthesized from the chemical bath deposition in the $TiCl_4$ solution. Although the stable low-temperature titania phase is anatase, the likely reasons for the formation of rutile is the use of $TiCl_4$ as a precursor which is prone to produce rutile nanoparticles on hydrolysis. The rutile large particles formed via chemical bath deposition adhere very strongly to the bottom mesoporous titania layer and hence no further calcination or sintering step is required for the formation of the scattering overlayer. Rutile-TiO_2 scattering particles can potentially be very effective in photovoltaic performance due to the high refractive index and excellent light scattering

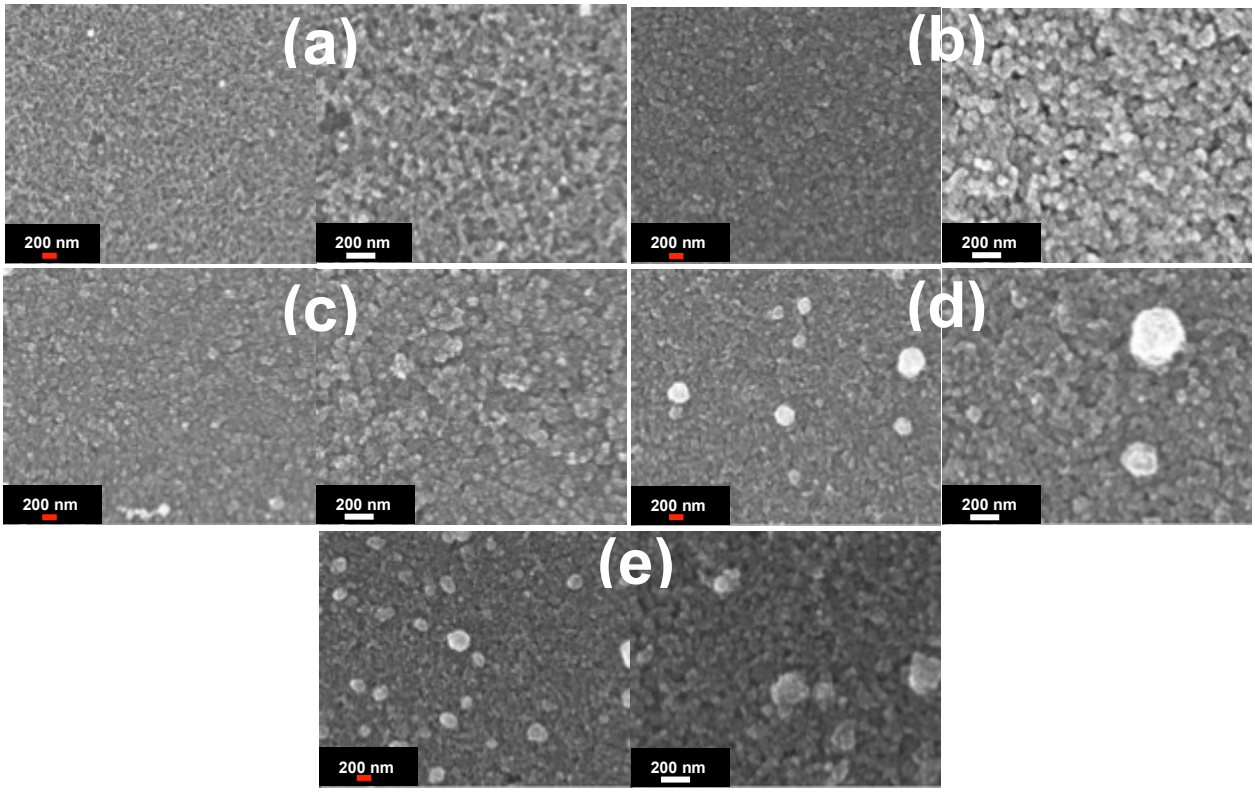

Figure 1. SEM images of the mesoporous TiO_2 films which were treated in a $TiCl_4$ solution with different concentrations (a) pristine, (b) 100 mM, (c) 200 mM, (d) 300 mM, and (e) 400 mM.

RSC Advances

ARTICLE

characteristics, which is a beneficial property for the perspective of effective light harvesting[22].

Optical spectroscopy

UV-vis absorption: Steady-state optical absorption spectra of TiO_2 films having been treated in a $TiCl_4$ solution with different concentrations are presented in Figure 2a. An enhancement in the absorption of the treated films can be observed while the fundamental absorption edge of TiO_2 appeared in the UV region at about 360 nm. We observed a slight deviation in the absorption slopes that are below the band edge at higher concentration of $TiCl_4$. Such deviations (without base line correction) could appear from strong light scattering, which originates from the formation of larger titania particles on the top surface of the mesoporous layer. This light scattering effect has been proved to be beneficial for light harvesting in DSC architecture. Consequently, a systematic design of cells by light scattering of the larger particles on the top surface can potentially improve the photovoltaic performance of DSCs.

Diffuse reflectance spectroscopy (DRS): To further confirm the light scattering behavior of $TiCl_4$ treated electrodes in different concentrations, we carried out diffuse reflectance spectroscopy measurement. Figure 2b shows the DRS spectra of the TiO_2 films prepared with various concentrations of $TiCl_4$ solution. In all measurements, the samples are irradiated from the side of the glass substrate on which the film is not deposited. When a beam of solar light passes the FTO glass and contacts with the TiO_2 films, the incident light is supposed to be reflected, scattered and transmitted within the films. In general, the part of incident light scattered within a film and returned to the surface is considered to be diffused reflectance[23]. It is evident that the light scattering capability of the TiO_2 electrodes that were treated in $TiCl_4$ solution with concentrations of 300mM and 400mM (e.g., TC300 and TC400) improved significantly compare to the pristine film in the spectral range from 300 to 800 nm. These can be ascribed to the formation of the large particles on the top surface of the mesoporous TiO_2 layer, which may act as light scattering centers. It is notable that the TC200 shows a slight higher scattering capability compare to the pristine film while TC100 has almost the same reflectance spectrum.

Photo thermal deflection spectroscopy

To investigate the influence of $TiCl_4$ treatment with different concentrations on trap states in TiO_2 mesoporous films, we performed photothermal deflection optical absorption

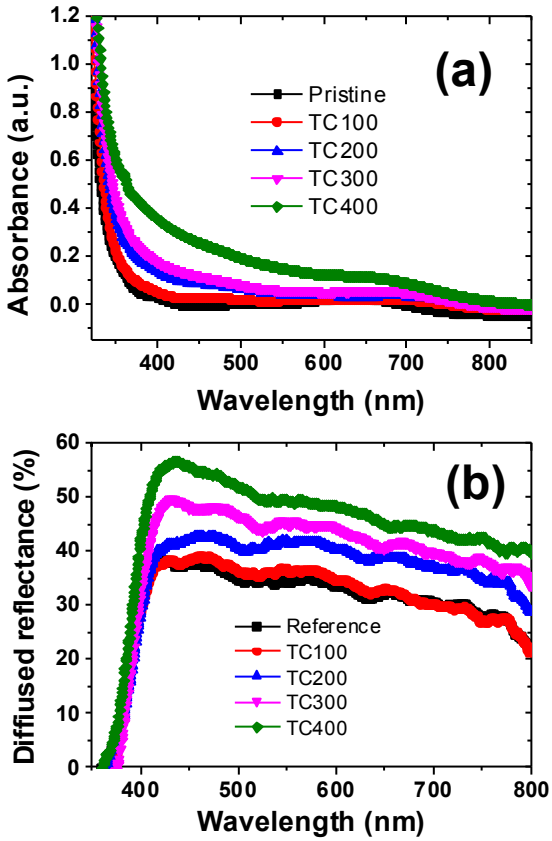

Figure 2. (a) Optical absorption spectra and (b) diffuse reflectance spectra of ms-TiO_2 films, unmodified (black curve) and $TiCl_4$ post treated films in different concentrations.

spectroscopy (PDS) measurement. PDS is a technique which allows us to probe with high sensitivity the sub- bandgap optical absorption, and thus the trap states due to under-coordinated surface Ti(IV) ions. The slope of the absorption at the band edge defines the Urbach energy, and provides a measure for the degree of disorder of a material[24]. In Figure 3a, we compare the PDS spectra of pristine and $TiCl_4$ treated ms-TiO_2 films in different concentrations deposited on quartz substrates. It is evident that $TiCl_4$ treatment significantly reduced the sub-bandgap absorption and increased the density of states (DOS) near the titania band edge in TiO_2 films which possibly can improve the charge transport within the mesoporous layer in a DSC configuration. It is notable that DOS for TC400 is the least among the treated titania films while TC200 and TC100 have higher DOS compare to TC300. This might potentially due to the formation of large size particles at higher $TiCl_4$ concentration, which can create some traps at the interfaces. In PDS spectra, the slope of the absorption at the band edge defines the Urbach energy, and provides a measure

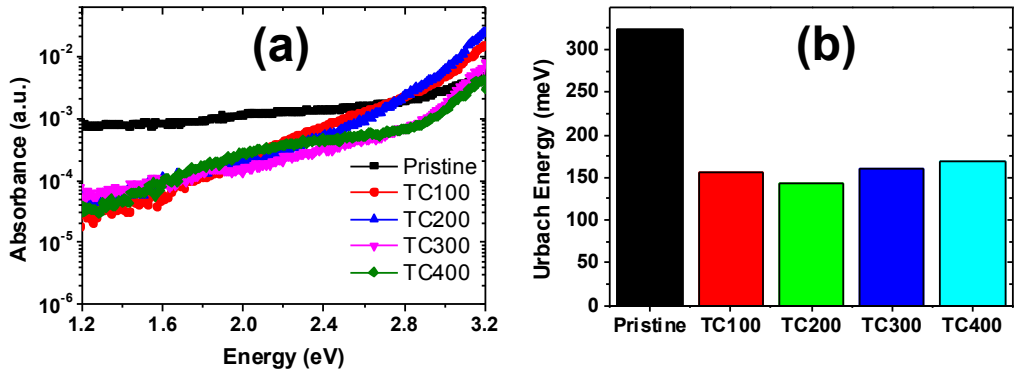

Figure 3. (a) PDS absorption spectra (b) Urbach energy of ms-TiO_2 films, unmodified (black curve) and $TiCl_4$ post treated films in different concentrations.

for the degree of disorder of a material. As shown in Figure 3b, the significant declines in the Urbach energy of $TiCl_4$ treated titania films in different concentrations (140-170 meV) compare to the pristine one (324 meV), further confirm that $TiCl_4$ treatment decreased the number of trap states.

Photovoltaic Performance

Photocurrent density–voltage (J-V) characteristics of the pristine and $TiCl_4$ treated with different concentrations titania based DSCs were measured under simulated air mass 1.5 global (AM1.5G) solar irradiation. The devices were fabricated based on the optimized procedure, which is explained in the Experimental Section. The J-V curves of the fabricated DSCs and the corresponding photovoltaic parameters such as short circuit current (J_{SC}), open circuit voltage (V_{OC}), fill factor (FF), power conversion efficiency (η) and the amount of dye adsorption are illustrated in Figure 4 and Table 1, respectively. The amount of dye loading was determined using a spectroscopic method by measuring the concentration of dye desorbed on the titania surface into solution of 0.1 molar NaOH. According to Beer–Lambert law, the amount of adsorbed dye was calculated with regard to the macroscopic geometric area of the TiO_2 film. The amount of dye adsorption for TiO_2 photoelectrodes followed a continuous decline by increasing the $TiCl_4$ concentration, which potentially because of the formation of larger particles at the surface of mesoporous titania layer.

Table 1. Summary of the photovoltaic parameters derived from J–V measurements of fabricated DSCs based on $TiCl_4$ treated titania photoanodes in different concentrations under illumination of 100 mW.cm^{-2}.

Type of sample	J_{SC} (mA.cm^{-2})	V_{OC} (mV)	FF	η (%)	Adsorbed dye (10^{-8} mol.cm^{-2})
Pristine	16.58	632	0.68	7.10	11.27
TC100	16.02	685	0.69	7.52	11.04
TC200	15.61	691	0.68	7.32	10.73
TC300	19.09	663	0.68	8.54	10.43
TC400	18.27	650	0.66	7.84	9.12

For the pristine cell, J_{sc} of 16.58 mA cm^{-2}, V_{oc} of 0.63 V, fill factor (FF) of 0.68, and PCE of 7.10% are achieved. It is evident that the J_{sc} decreased for the treated titania electrode in a $TiCl_4$ solution up to 200 mM while it reached the highest value of 19.09 mA cm^{-2} for the TC300. The initial decline of J_{sc} in TC100 and TC200 can be attributed to the lower dye loading (Table 1).

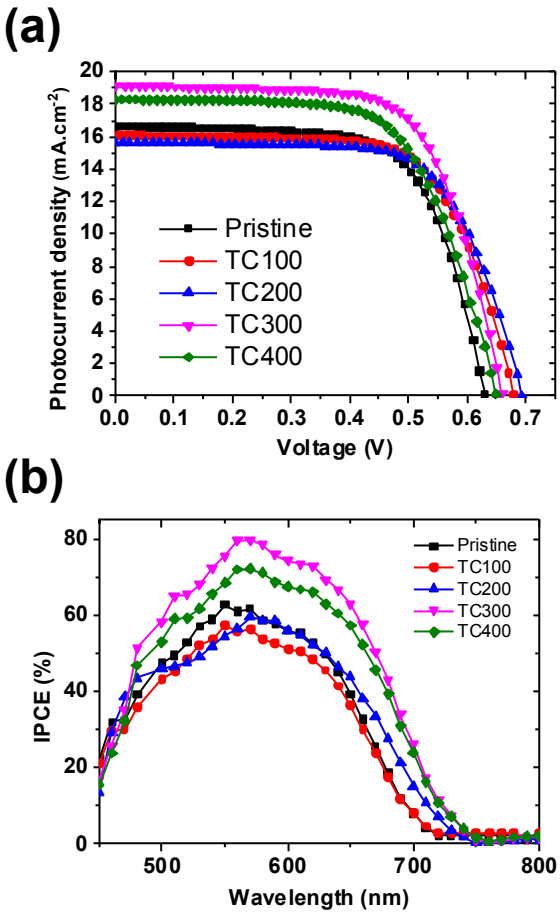

Figure 4. (a) Current–voltage characteristics of fabricated DSCs based on $TiCl_4$ treated titania photoanodes in different concentrations under illumination of 100 mW.cm^{-2} and (b) Incident photon-to-current efficiency (IPCE) spectra as a function of the wavelength of monochromatic light for the pristine, TC100, TC200, TC300 and TC400-based devices.

However, the J_{sc} improvement in TC300 can be explained due to the presence of larger titania particles on the top surface which act as scattering centers and improved the light harvesting efficiency (Figure 1 and Figure 2b). Further increase in the concentration of the $TiCl_4$ bath lead to a slight drop in the short circuit current (18.27 mA cm^{-2} for TC400), which is potentially because of the significant drop in the amount of adsorbed dye. The enhancement in current densities of DSCs based on $TiCl_4$ treated photoanodes is supported by the improvement in the incident photon to current conversion efficiency (IPCE) spectra shown in Figure 4b.

Moreover, a substantial enhancement in the V_{oc} of 0.68 V for TC100, 0.69 V for TC200, 0.66 V for TC300 and 0.65 V for TC400-based devices compare to 0.63 V for pristine solar cell was observed. This improvement of V_{oc} for the $TiCl_4$ treated electrodes can be attributed to the surface passivation effect of ms-TiO_2, which is consistent with the PDS results (Figure 3a) and the previous reports[25]. It is notable that the presence of large titania particles on the top surface in TC300 and TC400 cells can potentially increase the recombination rate due to the formation of new interfaces. The confluence of the aforementioned JV parameters leads to the PCE of 8.54% for TC300-based DSC as the optimum concentration of $TiCl_4$ solution compare to the 7.10% for the pristine cell.

Electrochemical impedance spectroscopy (EIS)

To study the impact of immersion of ms-TiO_2 electrodes in a $TiCl_4$ bath with different concentrations on the charge transport properties of fabricated DSCs, we employed EIS analysis. Figure 5 shows the EIS Nyquist plots of the complete devices under 100 mW.cm^{-2} and the equivalent circuit adopted to fit the Nyquist plots of DSCs. We used Z- view software to analyze the equivalent circuit and the resultant resistance values are summarized in Table 2.

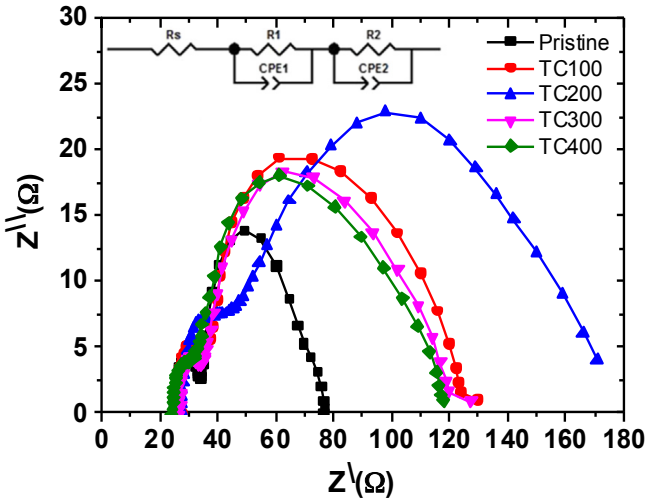

Figure 5. EIS Nyquist plots of complete titania based DSCs which were treated in controlled $TiCl_4$ chemical bath. The inset shows the corresponding equivalent circuit of a DSC used to fit the experimental data.

Table 2. Recombination and electronic transfer properties of the DSCs based on $TiCl_4$ treated titania photoanodes in different concentrations determined by fitting EIS spectra.

Type of Device	R_s (Ω)	R_1 (Ω)	R_2 (Ω)
Pristine	25.87	2.76	15.09
TC100	26.12	3.25	18.69
TC200	26.48	3.80	20.21
TC300	26.35	2.29	17.43
TC400	25.91	2.43	17.16

The resistance element R_s in the high-frequency region, which can be obtained from the first real intercept on the Nyquist plot, is responsible for the sheet resistance of conducting FTO. In this work, all DSCs have approximately a similar value of R_s (about 26 Ω) as the same FTO substrate is used to fabricate all the devices. The Nyquist plots exhibit two semicircles including a large semicircle at low frequency and a small one at high frequency. The small semicircle in the high-frequency range is attributed to the redox reaction at the platinum counter electrode, and the large semicircle in the low-frequency region takes into account the oxide/electrolyte interface[26,27]. From Table 2, it is evident that the charge-transfer resistance at the Pt/electrolyte interface (R_1) shows an opposite trend to the short circuit currents. This may be related to the concentration of I_3^- in the electrolyte. For restoring dye in the electrodes having higher photocurrent density, more I^- must be oxidized into I_3^-, which increases the concentration of I_3^- in the electrolyte. Therefore, DSCs with higher short circuit current has higher concentration of triiodide ions (I_3^-) in the electrolyte. According to the previous report, the reciprocal of charge-transfer resistance at the platinum/electrolyte interface is proportional to the square root of the I_3^- concentration within the electrolyte[28]. As a result, high concentration of triiodide ion (I_3^-) in electrolyte leads to the smaller resistance (R_1) of the counter electrode. Therefore, R_1 decreases with increasing the value of short circuit current.

From Figure 5, the large semicircle is evidently larger for all $TiCl_4$ treated cells compare to the pristine device, indicating that controlled $TiCl_4$ treatment diminish the recombination process at the oxide/electrolyte interface. This can be attributed to the formation of a barrier layer in the interface of TiO_2/Electrolyte which potentially can reduce the recombination rate. In addition, the recombination resistance values (R_2) are consistent with the open circuit voltage of the devices. It is notable that TC200 which showed the highest V_{oc} of 691 mV has the highest recombination resistance of 20.21 Ω compare to V_{oc} and R_2 of 632 mV and 15.09 Ω for the pristine device, respectively. As it is stated earlier, formation of large particles on the top surface of titania in TC300 and TC400 leads

to the decrees in the recombination resistance (R_2) due to the creation of new interfaces which ultimately leads to a decrease in V_{oc} of these devices. From this study, we illustrate a facile low-temperature route to fabricate a scattering layer consist of large nanocrystalline titania with rutile phase on the top surface of ms-TiO_2 in a DSC architecture which we observed a considerable improvement in the photovoltaic performance of the device. This photovoltaic enhancement is not only attributed to the improvement in the reflectance spectra, but also surface passivation of ms-TiO_2 is achieved at the same time which make this low temperature route unique in comparison to the previous reports[29,30] where an extra annealing step is needed to deposit a scattering layer.

Conclusions

In summary, we report a facile low-temperature route to form a scattering over-layer consist of large titania particles using controlled $TiCl_4$ post treatment. Experimental results demonstrate that the large scattering particles on the top layer work as efficient light scattering centers as confirmed by a significant improvement in the diffuse reflectance spectra of the treated films. In addition, we demonstrate an outstanding enhancement in the density of states of titania close to the band-edge upon $TiCl_4$ chemical bath treatment by photothermal deflection spectroscopy. We also showed that an optimum concentration of $TiCl_4$ bath is required as the dye loading of the titania films reduces at higher concentrations. Photovoltaic measurement of fabricated solar cells based on different concentrations of $TiCl_4$ post treatment shows an overall improvement in the open circuit voltage of the treated devices due to the surface passivation of mesoporous titania layer. This further confirmed by electrochemical impedance spectroscopy of the devices where the recombination resistance improved significantly upon the aforementioned treatment. Ultimately, the device having an optimum number of large particles on the top surface of photoanodes (TC300) showed the highest power conversion efficiency of 8.54% compare to PCE of 7.10% for the pristine solar cell.

Experimental section

Fabrication of mesoporous TiO_2 film: TiO_2 nanoparticles, with particle size in the range 15–30 nm and anatase structure, were prepared using a modified process analogous to our procedure reported previously[14]. The synthesis process was a combination of sol-gel and hydrothermal methods. Titanium isopropoxide (TIP) (purity 97%; Sigma Aldrich, Gillingham, U.K.) and 1-octanol (purity 99%; Merck, Darmstadt, Germany) were used as titanium precursor and the solvent, respectively. TIP was dissolved in 1-octanol to form a 0.55M transparent precursor solution. Deionized water, with molar ratio of [H_2O]:[Ti] = 3.3:1, was added slowly into the solution in order to form TiO_2 dispersion. It was kept magnetically stirred at a rotation speed of 480 rpm for 30 min to allow the hydrolysis and condensation reactions to occur. The prepared titania dispersion was transferred into a Teflon-lined stainless steel autoclave at a filling ratio of 70%. The autoclave was heated at 180°C for 4 h and subsequently cooled naturally to room temperature. The collected precipitates (i.e., anatase-TiO_2 nanoparticles) were washed with ethanol and deionized water several times and dried at 25°C.

TiO_2 pastes were prepared by mixing the synthesized TiO_2 nanoparticles, solvent, dispersing agents, and binders as it is reported elsewhere[31]. TiO_2 paste was spin coated on a fluorine doped tin oxide (FTO) substrate (2.0×1.5 cm^2 and with a sheet resistance of 7 Ω/sq). The spin coating parameters were controlled in order to obtain the desired thickness of 20 µm. The deposited TiO_2 films were annealed at 400°C for 2 hours in air atmosphere.

TiO_2 light scattering layer deposition: We employed a chemical bath deposition process, similar to the one previously used for dye-sensitized solar cells[32]. $TiCl_4$ was hydrolyzed in water, resulting in the formation of crystalline TiO_2 (rutile) particles. We use different concentrations of $TiCl_4$ in the chemical bath to control the size and agglomeration of the TiO_2 particles formed during the hydrolysis process. An aqueous stock solution of 2M $TiCl_4$ was diluted to different concentrations, the mesoporous titania were immersed into this solution followed by a heating in an oven at 70°C for 1 h in a closed vessel, and flushed with distilled water.

DSC Fabrication: The resulting TiO_2 electrodes were soaked in 0.5 mM ruthenium (II) dye (Ruthenium 535-bisTBA dye, or N719, Solaronix) solution (using ethanol as a solvent) for 18 h. The electrodes were washed with ethanol, dried and then immediately used for photovoltaic measurements. The redox electrolyte was composed of 0.6 M dimethylpropylimidazolium iodide, 0.1 M LiI, 0.05 M I_2 and 0.5 M 4-tertbutylpyridine in acetonitrile. Platinum-coated FTO substrate was prepared as a counter electrode. The platinum electrode was placed over the dye-adsorbed TiO_2 electrode, and the edges of the cell were sealed with sealing sheet (SX 1170-60, Solaronix). Sealing was accomplished by hot-pressing the two electrodes together at 120 °C. The redox electrolyte was injected into the cell through the small holes and sealed with a small square of sealing sheet.

Characterization and Measurements: The prepared scattering layers were characterized by scanning electron microscope (SEM) using FEI FEG XL30. The thickness of TiO_2 electrodes was measured with a Tensor Alpha-step Profiler. Diffuse reflectance spectroscopy (DRS) measurements of the films were recorded using an Avaspec-2048-TEC spectrometer. The optical absorption and concentrations of N719 in photoelectrodes were obtained by a UV–Vis spectrophotometer (6705 JENWAY). Photothermal Deflection Spectroscopy (PDS) measurements were performed on titania films prepared on quartz substrates, under identical conditions. PDS is a highly sensitive surface averaged absorption measurement technique that makes use of the heating effect on the sample upon absorption of absorbed monochromatic excitation, which creates a thermal gradient in front of the sample surface[33]. An inert liquid (Fluorinert FC-72, 3M Corporation) surrounding the sample enhances this thermal gradient. This gradient further results in a refractive

index gradient through which a continues wave laser is passed, skimming the sample surface. This laser beam gets deflected off its original path due to the presence of the refractive index gradient and this deflection is detected using a quadrant detector connected to a lock-in amplifier (Stanford Resarch SR830). The amount of deflection of the laser beam, which is proportional to the amount of absorbed is recorded as a function of the monochromatic excitation wavelength and by scanning through different wavelengths the complete absorption spectra is obtained.

Photovoltaic measurements of the fabricated solar cells were carried out, using Zahner Cimps pcs solar simulator (Zahner, Kronach, Germany) under the standard test conditions (i.e., irradiance of 100 mW/cm^2, AM 1.5 spectrum) with reference Si cell. The electrochemical impedance spectroscopy (EIS) measurements of the DSCs were recorded with a potentiostat/galvanostat (PGSTAT 302N, Autolab, Eco-Chemie, the Netherlands) under 100 mW/cm^2. EIS measurements were carried out under an open circuit potential with oscillation potential amplitudes of 10 mV from 0.01 to 106 Hz. The cells were studied in two-electrode configuration with 10 steps per decade above 66 Hz and lower limit of four. EIS spectra were then simulated using Z-view software.

The data underlying this paper are available at https://www.repository.cam.ac.uk/handle/1810/256769.

Acknowledgements

M. Abdi-Jalebi acknowledges Nava Technology Limited for the research grant. M. Abdi-Jalebi, Z. Andaji Garmaroudi and M. R. Mohammadi wish to thank the financial support from Iran Nanotechnology Initiative Council. M. Abdi-Jalebi gratefully acknowledges funding from Nyak Technology Limited. M. Abdi-Jalebi and R. H. Friend would like to acknowledge the support from EPSRC.

Notes and references

1 B. O'Regan and M. Grätzel, *Nature*, 1991, **353**, 737–740.

2 M. Wu, X. Lin, T. Wang, J. Qiu and T. Ma, *Energy Environ. Sci.*, 2011, **4Io**, 2308.

3 M. Graetzel, R. a J. Janssen, D. B. Mitzi and E. H. Sargent, *Nature*, 2012, **488**, 304–12.

4 S. Pan, Z. Yang, P. Chen, J. Deng, H. Li and H. Peng, *Angew. Chemie - Int. Ed.*, 2014, **53**, 6110–6114.

5 W. Zeng, L. Shu, Q. Li, S. Chen, F. Wang and X. M. Tao, *Adv. Mater.*, 2014, **26**, 5310–5336.

6 W. Wu, Y. Xu, H. Rao, C. Su and D. Kuang, 2014.

7 M. Abdi-Jalebi, M. R. Mohammadi and D. J. Fray, *J. Clust. Sci.*, 2014, **25**, 1029–1045.

8 N. Tétreault and M. Grätzel, *Energy Environ. Sci.*, 2012, **5**, 8506.

9 A. K. Chandiran, M. Abdi-Jalebi, A. Yella, M. I. Dar, C. Yi, S. A. Shivashankar, M. K. Nazeeruddin and M. Grätzel, *Nano Lett.*, 2014, **14**, 1190–1195.

10 M. Abdi-jalebi, A. K. Chandiran, M. K. Nazeeruddin and M. Gr, *Sci. Iran. F*, 2014, **21**, 2479–2484.

11 N. Massihi, M. R. Mohammadi, a. M. Bakhshayesh and M. Abdi-Jalebi, *Electrochim. Acta*, 2013, **111**, 921–929.

12 S. Mathew, A. Yella, P. Gao, R. Humphry-Baker, B. F. E. Curchod, N. Ashari-Astani, I. Tavernelli, U. Rothlisberger, M. K. Nazeeruddin and M. Grätzel, *Nat. Chem.*, 2014, **6**, 242–247.

13 X. Lai, J. E. Halpert and D. Wang, *Energy Environ. Sci.*, 2012, **5**, 5604.

14 Z. A. Garmaroudi and M. R. Mohammadi, *J. Sol-Gel Sci. Technol.*, 2015, **76**, 666–678.

15 W.-Q. Wu, Y.-F. Xu, H.-S. Rao, C.-Y. Su and D.-B. Kuang, *Nanoscale*, 2013, **5**, 4362–9.

16 L. Zhu, Y. L. Zhao, X. P. Lin, X. Q. Gu and Y. H. Qiang, *Superlattices Microstruct.*, 2014, **65**, 152–160.

17 T. G. Deepak, G. S. Anjusree, S. Thomas, T. a. Arun, S. V. Nair and a. Sreekumaran Nair, *RSC Adv.*, 2014, **4**, 17615.

18 X. Liu, M. Guo, J. Lin, X. Chen and H. Huang, *RSC Adv.*, 2014, **4**, 45180–45184.

19 L. Yang and W. W.-F. Leung, *RSC Adv.*, 2013, **3**, 25707.

20 P. Zhao, P. Cheng, B. Wang, S. Yao, P. Sun, F. Liu, J. Zheng and G. Lu, *RSC Adv.*, 2014, **4**, 64737–64743.

21 P. Cheng, P. Sun, S. Du, Y. Cai, X. Li, Z. Wang, F. Liu, J. Zheng and G. Lu, *RSC Adv.*, 2014, **4**, 23396.

22 A. K. Chandiran, M. Abdi-jalebi, M. K. Nazeeruddin and M. Gra, 2014, 2261–2268.

23 A. Furube, Z.-S. Wang, K. Sunahara, K. Hara, R. Katoh and M. Tachiya, *J. Am. Chem. Soc.*, 2010, **132**, 6614–6615.

24 M. Abdi-Jalebi, M. I. Dar, A. Sadhanala, S. P. Senanayak, M. Franckevičius, N. Arora, Y. Hu, M. K. Nazeeruddin, S. M. Zakeeruddin, M. Grätzel and R. H. Friend, *Adv. Energy Mater.*, 2016, **6**, 1502472.

25 H. Wang, B. Wang, J. Yu, Y. Hu, C. Xia, J. Zhang and R. Liu, *Sci. Rep.*, 2015, **5**, 9305.

26 F. Fabregat-Santiago, J. Bisquert, E. Palomares, L. Otero, D. Kuang, S. M. Zakeeruddin and M. Grätzel, *J. Phys. Chem. C*, 2007, **111**, 6550–6560.

27 Q. Wang, J.-E. Moser and M. Grätzel, *J. Phys. Chem. B*, 2005, **109**, 14945–53.

28 A. Hauch and A. Georg, *Electrochim. Acta*, 2001, **46**, 3457–3466.

29 W. Gan, H. Niu, X. Shang, R. Zhou, Z. Guo, X. Mao, L. Wan, J. Xu and S. Miao, *Phys. Status Solidi*, 2016, **213**, 994–1001.

30 A. M. Bakhshayesh, *Mater. Res. Bull.*, 2016, **73**, 268–275.

31 M. R. Mohammadi, R. R. M. Louca, D. J. Fray and M. E. Welland, *Sol. Energy*, 2012, **86**, 2654–2664.

32 S. Ito, P. Liska, P. Comte, R. Charvet, P. Péchy, U. Bach, L. Schmidt-Mende, S. M. Zakeeruddin, A. Kay, M. K. Nazeeruddin and M. Grätzel, *Chem. Commun. (Camb).*, 2005, 4351–4353.

33 A. J. Pearson, P. E. Hopkinson, E. Couderc, K. Domanski, M. Abdi-Jalebi and N. C. Greenham, *Org. Electron. physics, Mater. Appl.*, 2016, **30**, 225–236.